Adaptive Modular Neural Control for Online Gait Synchronization and Adaptation of an Assistive Lower-Limb Exoskeleton

Srisuchinnawong, Arthicha; Akkawutvanich, Chaicharn; Manoonpong, Poramate

Published in:
IEEE Transactions on Neural Networks and Learning Systems

DOI:
10.1109/TNNLS.2023.3263044

Publication date:
2024

Document version:
Accepted manuscript

Citation for pulished version (APA):
Srisuchinnawong, A., Akkawutvanich, C., & Manoonpong, P. (2024). Adaptive Modular Neural Control for Online Gait Synchronization and Adaptation of an Assistive Lower-Limb Exoskeleton. *IEEE Transactions on Neural Networks and Learning Systems*, *35*(9), 12449-12458. https://doi.org/10.1109/TNNLS.2023.3263044

Adaptive Modular Neural Control for Online Gait Synchronization and Adaptation of an Assistive Lower-Limb Exoskeleton

Arthicha Srisuchinnawong, Chaicharn Akkawutvanich, and Poramate Manoonpong, *Senior Member, IEEE*

***Abstract*—Gait synchronization has attracted significant attention in research on assistive lower-limb exoskeletons because it can circumvent conflicting movements and improve the assistance performance. This study proposes an adaptive modular neural control (AMNC) for online gait synchronization and the adaptation of a lower-limb exoskeleton. The AMNC comprises several distributed and interpretable neural modules that interact with each other to effectively exploit neural dynamics and adopt feedback signals to quickly reduce the tracking error, thereby smoothly synchronizing the exoskeleton movement with the user's movement on the fly. Taking state-of-the-art control as the benchmark, the proposed AMNC provides further improvements in the locomotion phase, frequency, and shape adaptation. Accordingly, under the physical interaction between the user and exoskeleton, the control can reduce the optimized tracking error and unseen interaction torque by up to 80% and 30%, respectively. Accordingly, this study contributes to the advancement of exoskeleton and wearable robotics research in gait assistance for the next generation of personalized healthcare.**

***Index Terms*—Assistive exoskeleton, human-robot interaction, motion assistance, neural control, neural network**

I. Introduction

Lower-limb exoskeletons have demonstrated promising results in assisting people during walking. They provide additional torque to support locomotion and therefore reduce the force required for locomotion. Walking with an exoskeleton on a level floor can result in a decrease of up to 79% in the applied force [1]. Exoskeletons of different types have been demonstrated to assist their users. Although multi-joint exoskeletons have been reported to outperform single-joint exoskeletons in terms of assistance, they have more complex control mechanism owing to their intertwined joint commands [2].

Typically, lower-limb exoskeleton control can be divided into three levels [3]: low-level control for motor position/torque control, mid-level control for trajectory generation, and high-level control for user intention and terrain prediction. Among these, the mid-level control is crucial to shaping the interaction of the exoskeleton with the user. It is further divided into two: (1) frequency/phase estimation and adaptation and (2) action/shape generation and adaptation [3]. Hence, most of the research on developing methods for accomplishing these two tasks.

Methods focusing on frequency/phase estimation and adaptation include event trigger-based control, Bayesian optimization-based control, and adaptive oscillator-based control. The event trigger-based control technique relies on foot pressure feedback for adaptation [4]. Hence, this technique can only adapt the frequency/phase of an exoskeleton in the stance phase where the feedback is presented, which results in the lack of continuous adaptation. The Bayesian optimization-based control technique is an alternative that allows continuous adaptation in both swing and stance phases. For example, the technique was applied to optimize lower-body exoskeleton walking gaits for user comfort over a high-dimensional parameter space related to frequency using user feedback [5]. Nevertheless, the technique requires several trials (at least 30 trails or $\gg$ 30 gait cycles) for the optimization process. In other studies, adaptive oscillator-based control was employed with various oscillator models, such as adaptive frequency oscillator (AFO) [6], adaptive Hopf oscillator [7], and particularly-shaped adaptive oscillator (PSAO) [8, 9]. These oscillators attempt to adapt certain parameters primarily based on trajectory feedback. Therefore, they require fewer trials (3–6 gait cycles) for each individual user.

Methods regarding action/shape generation and adaptation typically learn shape parameters. For example, dynamic movement primitive and hierarchical interactive learning (DMP-HIL) framework [10] was proposed to optimize both the mid-level shape and low-level model parameters online, yet the method required approximately 15 gait cycles to converge. Despite installing extra sensors on the user's leg and modeling the problem as leader-follower multi-agent reinforcement learning [11], the parameters of the neural network required a few walking cycles (i.e., $\approx$ 4 gait cycles) to converge. Therefore, these methods cannot be generally applied instantly to new users without spending time on training the shape parameters. To improve online shape adaptation speed, Qiu et al. [12] and Martinez et al. [13] proposed other shape adaptation techniques; however, the former only learned from stable gaits with a slow transition velocity, while the latter merely adapted the swing phase.

This paragraph of the first footnote will contain the date on which you have submitted for review.

A. S., C. A., and P. M. are with the Bio-inspired Robotics and Neural Engineering Laboratory, School of Information Science and Technology, Vidyasirimedhi Institute of Science and Technology, Rayong, Thailand (e-mail: arthichas_pro@vistec.ac.th, chaicharn.a_s17@vistec.ac.th, and poramate.m@vistec.ac.th).

A. S. and P. M. are also with the Embodied Artificial Intelligence and Neurorobotics Laboratory, SDU Biorobotics, The Mærsk Mc-Kinney Møller Institute, University of Southern Denmark, Odense, Denmark.

P. M. is the corresponding author.

Considering all the aforementioned aspects, the most advanced technique is the coupled cooperative primitives (CCP) [14], which integrated human-robot interaction terms based on the impedance model of encoder feedback into the DMP-HIL frameworks. This CCP-based control method has also been proven to outperform conventional DMP-HIL [10] on a physical exoskeleton in terms of interaction torque reduction. However, the method was unable to adapt to different frequencies owing to the frequency parameter being fixed to that of the recorded gait [10, 14].

Although the aforementioned methods for exoskeleton control are effective in their own way, in general, they cannot quickly adapt the combination of frequency, phase, and shape online within a gait cycle for individual users as well as different environmental conditions (refer to Table II). This limits the practical use of exoskeletons. To achieve instant online frequency, phase, and shape adaptations, including the generalization required for personalized gait assistance, this study proposes adaptive modular neural control (AMNC). We hypothesize that, by integrating sensory feedback, optimizing the tracking error (the error between position command and position feedback), and adapting the neural dynamics embedded in the neural control, the AMNC can simultaneously adapt the frequency, phase, and shape of the control signals instantly online, thereby achieving a lower tracking error for effective personalized gait assistance within a gait cycle. Hence, when using AMNC, the exoskeleton can be aware of the user's intention based solely on the tracking error, and effectively assist its user by reducing the interaction torque (the user's force resisting the exoskeleton's movement). In general, the key contributions of this work are as follows:

- The AMNC of an assistive lower-limb exoskeleton that can generate and spontaneously adapt its frequency and trajectory shape online within a gait cycle while maintaining a human-like gait. In principle, the AMNC can be considered as the mid-level feedback control that adopts i) modular neural networks as the control model, ii) joint positions as sensory feedback, and iii) gradient-based adaptation (GA) and couple cooperative primitive-based adaptation (CA) networks as online error-based trajectory adaptation mechanisms. Instead of adopting direct feedback multiplied by gains for adaptation as in typical feedback control, the GA and CA translate feedback into adaptation feedback signals using impedance model and gradient descent techniques, thereby resulting in fast adaptation and generalization to different users and different environmental conditions (e.g., walking on a treadmill with varying slope angles).
- Proposed novel strategy that solely optimizes the positional tracking error of an assistive lower-limb exoskeleton, enabling the exoskeleton to automatically synchronize the walking phase and trajectory shape, thereby reducing the average interaction torque.

This article is organized as follows. Section II provides information on the exoskeleton system. Subsequently, Section III describes the modular neural control and the design concepts. Next, Section IV presents the experimental setup and results. Finally, Section V discusses the results and summarizes the contributions of this research.

II. Assistive Lower-limb Exoskeleton

In this study, Technaid's lower-limb exoskeleton [15] is employed, as illustrated in Fig. 1(a). The exoskeleton has six active joints, including right/left hips (RH/LH), right/left knees (RK/LK), and right/left ankles (RA/LA), operating on the sagittal plane. A flexible torso allows the user to swing the legs sideways within a small range; hence, two crutches are provided to the user for lateral support. A backpack with batteries and a portable PC (Intel® NUC7i7BNH), functioning as the onboard controller, are included in the system.

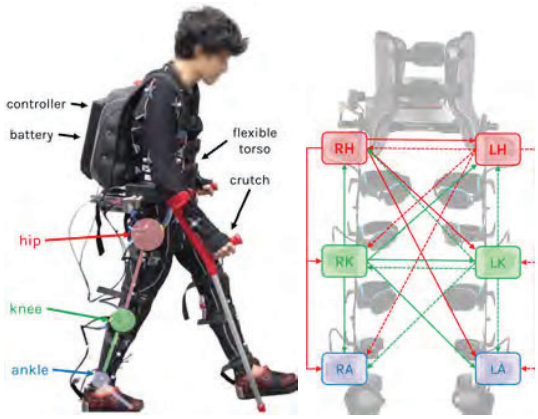

(a) (b)

Fig. 1: (a) Hardware of the exoskeleton system, including one Technaid Exo-H3 (the latest version of Technaid's lower limbs robotic exoskeleton) [15], two crutches and a backpack with a controller and batteries. (b) Control software of the exoskeleton system comprises six neural joint modules and symmetric coupled CPG adaptation signals. The interconnections of adaptation signals are introduced to the system to adapt all CPGs jointly and guarantee anti-phase motion between the left and right legs.

There are two sensors at each joint, including a position encoder and torque sensor. The encoder is for low-level position control and is adopted as sensory feedback to the controls for tracking error calculation, whereas the torque sensor is only employed in the evaluation of the interaction torque, which is unseen by both the AMNC and benchmark.

III. Adaptive Modular Neural Control

The proposed modular neural control comprises six neural joint modules with interconnected feedback loops, as illustrated in Fig. 1(b). Hip and knee modules share their feedback pathways to all modules, while ankle modules only receive adaptation signals from the others. This coupling structure with bidirectional hip and knee feedback pathways is adopted to ensure a 90^o phase difference between the left

and right legs[1]. The structure of each module in this research is designed as presented in Fig. 2 to generate joint rhythmic motion, synchronization, and adaptation. A joint module comprises six sub-modules: a central pattern generator network (CPG), a radial basis function network (RBF), a forward dynamics network (FD), two gradient-based adaptation networks (GAs), and a coupled cooperative primitive-based adaptation network (CA). The first three sub-modules (i.e., CPG, RBF, and FD) are for generating a rhythmic joint trajectory for low-level position control, while the others (i.e., GAs and CA) are for adaptation. To the best of our knowledge, an integration of the six modules for individual joint control with interconnected feedback loops for joint synchronization and fast adaptation has not yet been presented (refer to Table SI in the supplementary material).

All neurons in the AMNC are modeled as discrete-time neurons, updating at 30 Hz, according to:

$$n_j[t] = g(\sum_i w_{ji} n_i[t]), \tag{1}$$

where $n_i[t]$ denotes the output of neuron n_i at timestep t, w_{ji} denotes the weight of the connection from the pre-synaptic neuron n_i to post-synaptic neuron n_j, and $g()$ denotes the activation function.

A. Neural Modules for Trajectory Generation

1) Adaptable Central Pattern Generator (CPG): The role of the CPG, as illustrated in Fig. 2, is to function as a rhythmic phase system (i.e., C1 and C2) with adaptability and drive the exoskeleton. To achieve this, we extended an SO(2) neural oscillator[2] [16] by introducing CPG adaptation signals (i.e., δ^x_{C1} and δ^x_{C2} in Eq. 2 and Eq. 10) to enable it automatically adapt to user motion. Therefore, the modified SO(2) neural oscillator functions as the adaptable CPG for phase, frequency, and shape adaptation of each joint module. Note that the simultaneous phase, frequency, shape adaptation cannot be achieved by the original SO(2) oscillator. The dynamics of the adaptable CPG is governed by:

$$\begin{bmatrix} C_1[t] \\ C_2[t] \end{bmatrix} = tanh\left(\begin{bmatrix} C^*_1[t] \\ C^*_2[t] \end{bmatrix} + \sum_x \begin{bmatrix} \delta^x_{C1}[t] \\ \delta^x_{C2}[t] \end{bmatrix} \right), \tag{2}$$

$$\begin{bmatrix} C^*_1[t] \\ C^*_2[t] \end{bmatrix} = \begin{bmatrix} w_{11} & w_{12} \\ w_{21} & w_{22} \end{bmatrix} \begin{bmatrix} C_1[t-1] \\ C_2[t-1] \end{bmatrix}, \tag{3}$$

where $C_j[t]$ denotes the output of the neuron C_j at timestep t, and w_{ji} represents the weight of the connection from C_i to C_j, with w_{11} and w_{22} being 1.0087, w_{12} 0.0497, w_{21} -0.0497 [16], while $\delta^x_{Cj}[t]$ denotes the CPG adaptation signals from the GA of joint x passing to C_j at timestep t, and $tanh()$ denotes the hyperbolic tangent activation function.

The dynamics of the CPG is constrained by the activation function to produce two sinusoidal-like phase signals that oscillate between -1.0 and 1.0, as presented in the third row of Fig. 4. It guarantees that the phase oscillating signals and output trajectory are bounded during adaptation. The CPG outputs then function as the phase signals that repeatedly drive a radial basis function network (RBF) [17].

2) Radial Basis Function Network (RBF): Receiving the phase signals from the CPG, the RBF [17] presented in Fig. 2 maps the periodic phase signals to the forcing term (f), pushing the dynamics of the system toward the desired physical kinematic profile. The forcing term is generated by a weighted combination of the multiple Gaussian kernel, according to:

$$K_i[t] = e^{-\frac{1}{\sigma}\sum_{j=1}^{j=2}(C_j[t]-R_{ji})^2}, \tag{4}$$

$$f[t] = \sum_{i=1}^{32} w_{fi} K_i[t], \tag{5}$$

where $f[t]$ and $C_j[t]$ denote the output of f and C_j at timestep t, $K_i[t]$ denotes the output of K_i (i.e., an RBF kernel) at timestep t, w_{fi} denotes the weight of the connection from K_i to f, R_{ji} when $i \in [1, 32]$ denote the 32-point interpolation of the non-adapted $C_j[t]$ acting as the centers of the RBF, while σ denotes the scaling gain. According to this 32-point interpolation, we utilized 32 kernels/RBF neurons to cover the CPG signals. It should be noted that in this study, the number of interpolation points and scaling gains were empirically selected to 32 and 0.01 to optimize the output shape and smoothness.

The connection weights between K_i and f denote the key factors that determine the forcing terms. Consequently, they were trained to imitate the default joint trajectories provided by the manufacturer of Exo-H3 [15] via offline gradient-based optimization [18]:

$$w_{fi} \leftarrow w_{fi} - \frac{\rho}{T}\frac{\partial}{\partial w_{fi}} \sum_{t=0}^{T} (\bar{\theta}[t] - \theta[t])^2, \tag{6}$$

where w_{fi} denotes the weight of the connection from K_i to f, T denotes the number of timestep (here T = 128) in the target joint trajectory $\bar{\theta}[t]$ (obtained from the manufacturer of Exo-H3), $\theta[t]$ denotes the trajectory command generated from the AMNC at time t, and ρ denotes a learning rate empirically set to 0.01.

The optimization process was terminated after the mean square error was below 1e-4 rad. It should be noted that the optimization was performed only once, and the weights remained the same with all subjects throughout the trials. This guarantees the generation of the human-like gait pattern, while the CA and GAs are responsible for the online adaptation.

The produced forcing term is then passed through the forward dynamics network (FD) to drive the forward dynamic model of the exoskeleton toward the desired motion.

[1]Notably, we observed that the ankle joints exhibited the lowest absolute tracking error compared to the hip and knee joints, when testing with the CCP baseline approach (refer to Fig. 7). Hence, we hypothesize and demonstrate that large tracking hip and knee errors are adequate for assessing the quality of the user and exoskeleton interactions and can be employed for gait improvement and adaptation.

[2]The SO(2) neural oscillator is a special type of 2-neuron network where its weight matrix corresponds to an element in the Special Orthogonal group in two dimensions SO(2) [16].

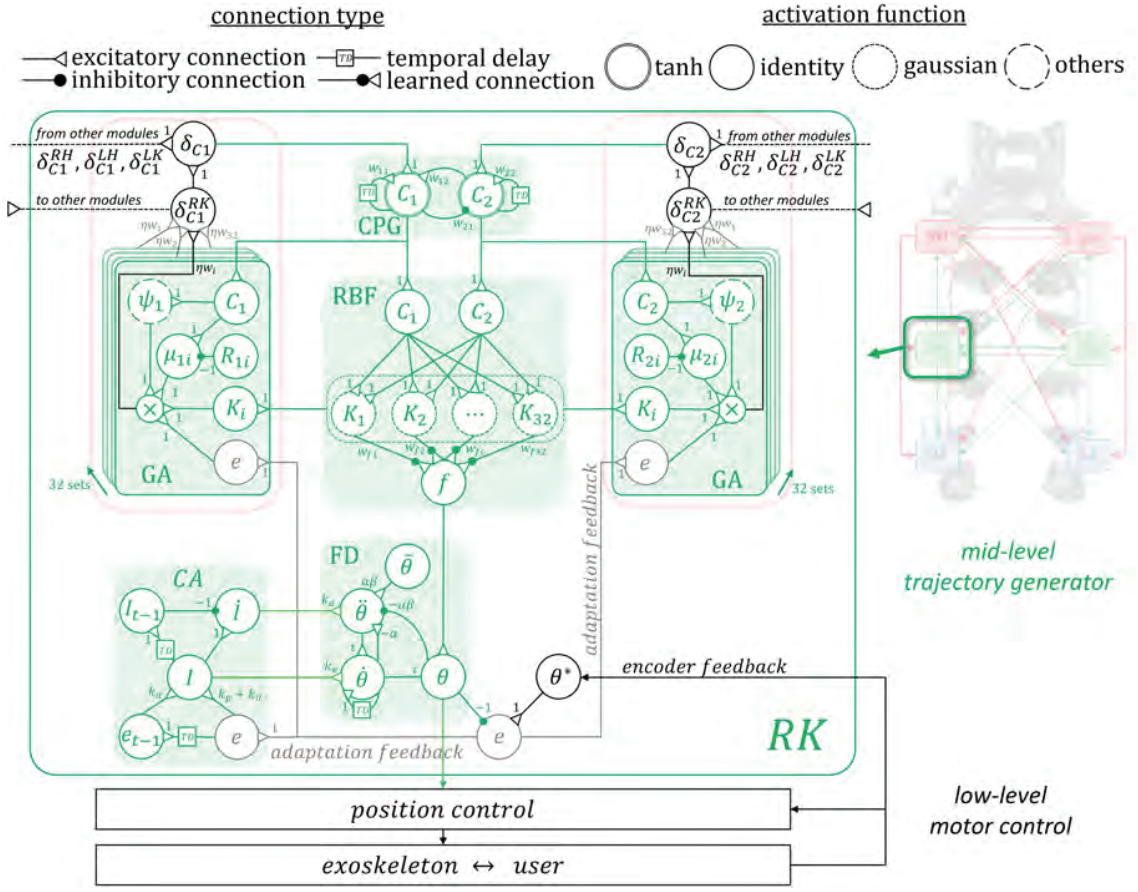

Fig. 2: Adaptive modular neural control (AMNC) of the RK joint module. The parameters of the control (i.e., connection weights) and pseudocode are summarized in Table SII and Algorithm S1 in the supplementary material. AMNC functions as the mid-level control for continuous trajectory generation and online adaptation. The low-level motor position control is implemented on the Exo-H3 controller [15]. Note that the GA parts highlighted by the red boxes, newly introduced here, are yet to be included in the benchmark CCP-control.

3) Forward Dynamics Network (FD): To avoid integrating the fitting error of the RBF, in the FD, the generated forcing term was applied to the position level according to Eqs. 7–9, to drive the forward dynamic model of the exoskeleton toward the desired direction. It should be noted that applying the forcing terms at the acceleration or velocity levels integrates the fitting error in every timestep, which results in a poor fitting performance [19], as illustrated in Fig. S1 in the supplementary material.

$$\ddot{\theta}[t] = \alpha\left(\beta(\bar{\theta}[t-1] - \theta[t-1]) - \dot{\theta}[t-1]\right) + k_a\dot{I}[t], \quad (7)$$

$$\dot{\theta}[t] = \dot{\theta}[t-1] + \tau\ddot{\theta}[t] + k_v I[t], \quad (8)$$

$$\theta[t] = f[t] + \tau\dot{\theta}[t], \quad (9)$$

where θ[t], $\dot{\theta}[t]$, $\ddot{\theta}[t]$ denote the output of θ, $\dot{\theta}$, and $\ddot{\theta}$ at timestep t, respectively, $\theta[t]$ is the position profile passing to the low-level position control at timestep t, $f[t]$ denotes the forcing term at timestep t, $\bar{\theta}[t]$ denotes the target joint trajectory at timestep t, τ denotes the time constant, $I[t]$ and $\dot{I}[t]$ denote the impedance-based adaptation signals from the CA at timestep t, and k_v, k_a, α, and β denote the gains. To ensure the fastest response time for the adaptation with no oscillation, these gains were empirically selected as 2.5, 1.8, 1.0, and 4.0, respectively.

B. Neural Modules for Trajectory Adaptation

1) Gradient-Based Adaptation Network (GA): The GA receives the tracking error as its input and converts it to the adaptation signals passing to the CPG (i.e., δ^x_{C1} and δ^x_{C2}). The conversion design is based on the gradient-based optimization: δ^x_{C1} and δ^x_{C2} are produced from the gradients of the tracking error relative to C^*_1 and C^*_2 according to:

$$\begin{bmatrix}\delta^x_{C1}[t]\\ \delta^x_{C2}[t]\end{bmatrix} = -\eta\begin{bmatrix}\frac{\partial e[t]^2}{\partial C^*_1}\\ \frac{\partial e[t]^2}{\partial C^*_2}\end{bmatrix}, \quad (10)$$

$$\begin{bmatrix}\delta^x_{C1}[t]\\ \delta^x_{C2}[t]\end{bmatrix} = \sum_{i=1}^{32}\eta w_{fi}[t]K_i[t]e[t]\begin{bmatrix}\mu_{1i}[t]\psi_1[t]\\ \mu_{2i}[t]\psi_2[t]\end{bmatrix}, \quad (11)$$

$$e[t] = \theta^*[t] - \theta[t], \quad (12)$$

$$\mu_{ji}[t] = C_j[t] - R_{ji}, \quad (13)$$

$$\psi_j[t] = 1 - C^2_j[t], \quad (14)$$

where $\delta^x_{Cj}[t]$ denotes the CPG adaptation signal from joint x passing as the input to C_j at timestep t, η denotes the adaptation gain, which is empirically selected as 0.2 to achieve the fastest adaptation response without oscillation, $e[t]$ denotes the output of e (the tracking error) at timestep t, C^*_1 and C^*_2 are the variables in Eq. 3, $K_i[t]$, $\mu_{ji}[t]$, and $\psi_j[t]$ denote the output of neuron K_i, μ_{ji}, and ψ_j at timestep t, respectively, $\theta[t]$ and $\theta^*[t]$ denote the control command and position feedback at timestep t, respectively, and R_{ji} denotes the variable in Eq. 4. Note that j denotes the index of the CPG signal, while i denotes the index of the RBF kernel.

To maintain antagonistic motion, all CPGs are adapted jointly. In other words, δ^x_{C1} and δ^x_{C2} from each joint module are summed together and fed to C_1 and C_2, respectively, according to Eq. 2. This creates the feedback pathway presented in Fig. 1(b) and the adaptation signal in the fourth row of Fig. 4.

2) Couple Cooperative Primitive-Based Adaptation Network (CA): To establish the state-of-the-art CCP [14] as the benchmark control, the AMNC is equipped with the CA to convert the tracking error to the adaptation signals passing to the FD according to:

$$I[t] = k_p(\theta^*[t] - \theta[t]) + k_d(\dot{\theta}^*[t] - \dot{\theta}[t]), \quad (15)$$

$$I[t] = (k_p + k_d)e[t] - k_d e[t-1], \quad (16)$$

$$\dot{I}[t] = I[t] - I[t-1], \quad (17)$$

where $I[t]$ and $\dot{I}[t]$ denote the output of I and $\dot{I}$, which represent the impedance-based adaptation signals, at timestep t; $e[t]$ denotes the output of e at timestep t, $\theta[t]$ and $\dot{\theta}[t]$ denote the target position (i.e., control command) and velocity at timestep t, respectively; $\theta^*[t]$ and $\dot{\theta}^*[t]$ denote the feedback position and velocity at timestep t, respectively; and k_p and k_d denote the gains empirically selected as 1.2 and 0.8 to achieve the fastest adaptation response without oscillation. It should be noted that Eq. 15 is equivalent to Eq. 16. Examples of the adaptation signals from the CA are presented in the second row of Fig. 4.

IV. Experiments and Results

In this study, two adaptive controls, the proposed AMNC and state-of-the-art CCP-based control [14], were evaluated on five recruited subjects with different experience, weights, and heights under the neural control framework. Different subjects were recruited to ensure alternative walking profiles for investigating the adaptability of each control method. Each subject was asked to perform six trials: three with the CCP control and three with the AMNC. In each trial, the subject walked under the assistance of the exoskeleton for 20 m over 20 gait cycles. All trials began once the subject put on the exoskeleton because no parameter was altered. A slow walking frequency (i.e., approximately 0.2 Hz) was selected to ensure safety. The subject's ID, experience, weight, height, and trial sequence are presented in Tables. I.

In the first experiment (section IV-A), the AMNC and CCP control are evaluated according to their adaptability to the user's phase, frequency, and shape in simulation. In the second experiment (section IV-B), the two controls are compared in terms of signals, including control command, phase system, and adaptation signals. In the third experiment (section IV-C), the two controls with multiple users are physically compared in terms of online adaptation to multiple gait features. Finally, in the last experiment (section IV-D), the two controls are compared in terms of tracking error and interaction torque reductions.

TABLE I: Subject's ID, weight, height, experience, and trial sequence. Note that "c" and "a" denote the trials with the CCP control and AMNC, respectively.

ID	A	B	C	D	E
weight	61 kg	55 kg	48 kg	68 kg	63 kg
height	170 cm	178 cm	157 cm	169 cm	178 cm
experience (before)	>5 times	3 times	2 times	2 times	0 times
sequence	c,a,a,c,c,a	c,a,a,c,c,a	a,c,c,a,a,c	a,c,c,a,a,c	c,a,a,c,c,a

A. Experiment I: Phase, Frequency, and Shape Adaptation in Simulation

The first experiment attempts to test and compare the AMNC and CCP-based benchmark control in terms of their adaptability to the user's phase, frequency, and amplitude in a CoppeliaSim simulation [20]. The simulation comprises the exoskeleton and a user that does not change their gait pattern. The exoskeleton interacts with the user via the straps, as illustrated in Fig. 3(a). The objective of the exoskeleton system is to adapt itself to the user gait pattern on the fly, thereby reducing the tracking error. This experiment was performed 10 times with each control, and the obtained average along with the range is presented in Fig. 3(b–d).

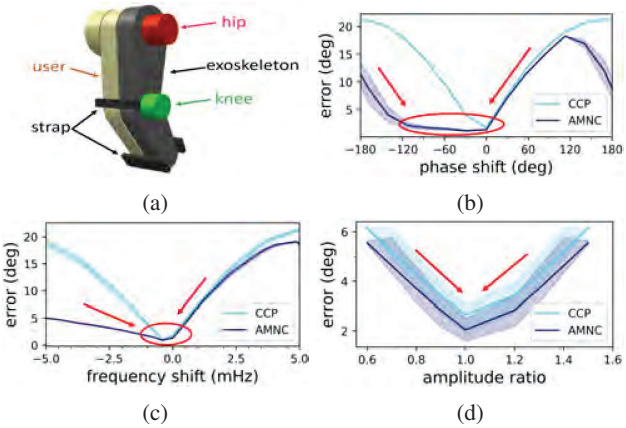

Fig. 3: (a) CoppeliaSim simulation [20] of the exoskeleton system and the average tracking error at the next gait cycle when the exoskeleton and user have different degrees of (b) phase (i.e., phase shift), (c) frequency (i.e., frequency shift), and (d) amplitude/shape (i.e., amplitude ratio).

The results presented in Fig. 3(b–d) indicate that the proposed AMNC outperforms the benchmark CCP-based

control in all the test conditions. In addition, it produces a pattern with a lower average tracking error. This indicates that the proposed AMNC exhibits a greater adaptability to user gait pattern than the benchmark. However, an asymmetric pattern can be observed in the results owing to the local minimum problem in gradient-based optimization [18]. Because both methods do not learn frequency and shape parameters but generate adaptation signals based on neural dynamics and signal processing, they can quickly adapt to the user's gait pattern and maintain minimal tracking error within a certain range (refer to the red circles in Fig. 3(b–c)).

B. Experiment II: Signal Comparison and Online Adaptation

The second experiment attempts to investigate how the adaptation signals affect the phase system, CPG signals, and control command online. In the first step, subject B utilized the exoskeleton with CCP and AMNC. During this step, the control command, feedback, and activities of the CPGs were recorded.

According to the results of the AMNC presented in Fig. 4, the adaptation signals (in the fourth row) can accelerate and deaccelerate the phase system (in the third row), making each point in the trajectory (in the first row) shift toward the feedback and assisting the CA adaptation signal (in the second row). Moreover, the adaptation was achieved in real time, which implies that the exoskeleton could adapt immediately using the data from the previous timestep. For example, at approximately 30% of the gait cycle (see Fig. 4), the AMNC feeds a positive adaptation signal ($\delta_{C1}[t]$) to C_1 (solid line), deviating from the non-adapted signal of the CCP. Consequently, the phase system ($C_1[t]$) accelerates, causing the left hip trajectory from the AMNC to change toward the feedback (black dashed line) and become closer to the feedback than the left hip trajectory from the CCP. With this mechanism, the adaptation signal from the CA (CA output) of the AMNC is assisted by the GA adaptation signal (GA output); hence, it is lower than the CA output of the benchmark CCP control. It should be noted that the magnitude of the adaptation signal has a non-linear relationship with the trajectory adaptation, and it is decided automatically by the CA and GA.

C. Experiment III: Online Adaptation During Human-Exoskeleton Interaction

The third experiment attempts to quantitatively validate the ability to adapt the trajectory profile along with the frequency/phase in a physical exoskeleton under human-exoskeleton interaction or two-way synchronization (i.e., the adaptation from both the exoskeleton and subject). This experiment was designed under the assumption that less adaptable control would produce a similar trajectory profile among the subjects, as the exoskeleton exhibits minor adaptation, whereas more adaptable control would adapt well to the subject's natural locomotion phase, frequency, and shape. This would result in a wider range of the frequency, phase, and shape and more personalized gait assistance.

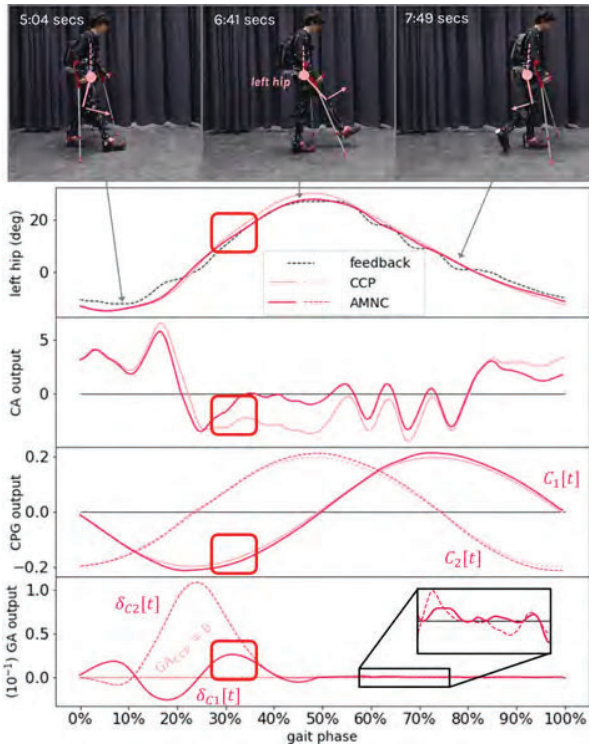

Fig. 4: Screenshots from the video of the walking experiment (https://youtu.be/WwdrFzYO8fY), control command, feedback trajectories, CPG outputs, and adaptation signals from the CA and GA of the left hip module. The signals were evaluated with the AMNC and CCP control. The black dashed line denotes the positional feedback, whereas the dark red solid and dash lines represent the signals from the proposed AMNC; in addition, the light red solid and dash lines represent the signals from the CCP control. Note that the GA signals of the benchmark CCP control remained at zero as they did not have the gradient-based adaptation mechanism. Another example from the knee module is available in Fig. S6 in the supplementary material.

To investigate these aspects, all subjects were asked to use the exoskeleton with the AMNC and CCP. The obtained results were then compared in terms of phase, frequency, and shape. Phase difference was calculated from the difference between the adapted exoskeleton control signals (either from the AMNC or CCP control) and non-adapted control signals, as expressed in Eq. 18, while locomotion frequency was estimated from the period of the control signal, as expressed in Eq. 19. The shape difference score is calculated from the absolute difference between the adapted control command (either from the AMNC or CCP control) and the non-adapted control command, as expressed in Eq. 20.

$$\Delta C[t] = \sqrt{(C_1[t] - C_1'[t])^2 + (C_2[t] - C_2'[t])^2} \tag{18}$$

$$f_i = \frac{1}{T_i}, \tag{19}$$

$$\Delta\theta[t] = |\theta[t] - \theta'[t]|, \tag{20}$$

where $\Delta C[t]$ and $\Delta\theta[t]$ denote the phase and shape

difference scores at timestep t, f_i denotes the frequency of the i^{th} gait cycle, $C_1[t]$ and $C_2[t]$ denote the adapted CPG signals at timestep t, $C_1'[t]$ and $C_2'[t]$ denote the non-adapted CPG signals at timestep t, T_i denotes the period of the CPG signals at gait cycle i, and $\theta[t]$ and $\theta'[t]$ denote the adapted and non-adapted control signals at timestep t where the signals are in the same phase.

Regarding phase and frequency adaptability, the results presented in Fig. 5(a) indicate that, because the adaptation to the subject's motion changes every gait cycle, the exoskeleton control signals from the AMNC deviate more from the non-adapted signals than those from the CCP control with higher phase difference scores of approximately 800%, as illustrated in Fig. 5(a) (p-value $<$ 0.05, Mann–Whitney U test). Fig. 5(b) also indicates that the locomotion frequency from the AMNC is approximately 3% higher than that from the CCP control (p-value $<$ 0.05, Mann–Whitney U test). These results indicate that the AMNC can adapt the phase and frequency of the control signals in a broader range than that of the CCP control. Furthermore, with the AMNC, the phase difference and walking frequency vary among the subjects. The more experience the subject has, the better the performance of the synchronization between subject and exoskeleton is. This provides evidence to support that the AMNC can adapt to different users.

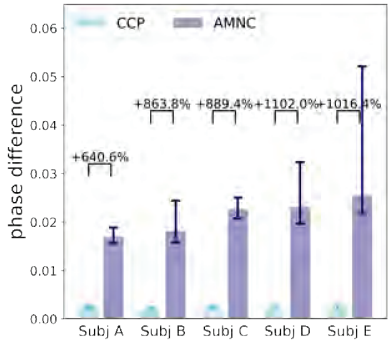

(a)

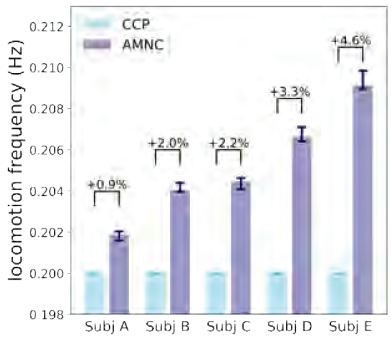

(b)

Fig. 5: (a) Phase difference and (b) locomotion frequency of the subjects using the exoskeleton with the AMNC (dark blue) and the benchmark CCP control (light blue). Note that the error bars represent the minimum and maximum values.

Regarding shape adaptability, the results in Fig. 6 indicate that, compared with the CCP control, the shape difference scores of the AMNC are approximately 20% higher in all subjects and all joints (p-value $<$ 0.05, Mann–Whitney U test).

D. Experiment IV: Tracking Error and Interaction Torque

As an evidence of shape and frequency adaptation, the final experiment compares the degree to which the exoskeleton with the AMNC and benchmark CCP control can assist and adapt to the users. Using the data recorded in previous experiments, the comparison was conducted via the analysis of the tracking error and interaction torque. The tracking error is the optimized variable in the AMNC and represents the degree of synchronization, while the interaction torque is the unseen variable that represents the degree of conflict movement. It should also be noted that high interaction torque can be interpreted as more conflict movement and less assistance.

According to the results of the tracking error presented in Fig. 7, the proposed method can further reduce the tracking error from the CCP control by 60–80% in the hip joints, 20–40% in the knee joints, and 30–40% in the ankle joints (p-value $<$ 0.05, Mann–Whitney U test). Synchronization improved with all the subjects, especially for the inexperienced user. Therefore, the results confirm that the AMNC can further reduce the optimized value even if the interaction between the user and exoskeleton is included.

According to the results presented in Fig. 8, when comparing the interaction torques of the AMNC and CCP control, the reduction in tracking error leads to a decrease of 7–30% in the hip joints, 10-30% in the knee joints, and 3–13% in the ankle joints (p-value $<$ 0.05, Mann–Whitney U test). Exhibiting a similar trend to the tracking error, the greatest assistance improvement occurred with the inexperienced user, while all subjects received reduced conflicted movement and improved locomotion assistance using the AMNC.

V. Discussion and Conclusion

Currently, most existing methods can achieve either trajectory frequency/phase adaptation [7] or shape adaptation [10, 11, 14] (see Table II). However, this study demonstrates that in addition to controlling the output frequency/phase, providing feedback to the oscillator functioning as the phase system can also control the output shape simultaneously. Nevertheless, the feedback loop must be carefully designed to achieve this. One approach presented in this study is to employ gradient optimization (section III-B1). The feedback passing to a certain adaptable variable should be an adaptation gain multiplied by the partial derivative of the value to be optimized (i.e., tracking error) relative to the adapted variable (i.e., phase system), as expressed in Eqs. 10–14.

With such an approach, the AMNC of an assistive lower-limb exoskeleton is proposed, to synchronize the exoskeleton's motion to that of the user, while solely focusing on the reduction in tracking error. Consequently, the

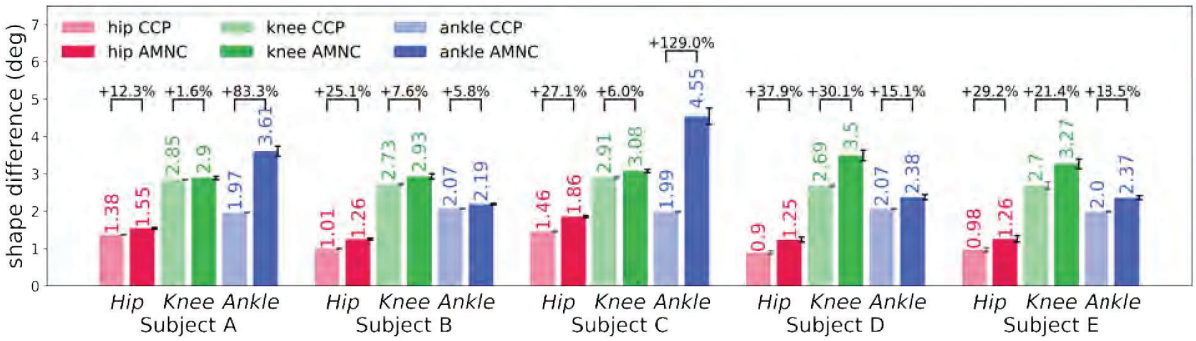

Fig. 6: Shape difference score of different joints (i.e., hip, knee, and ankle), evaluated on five subjects under two controls (i.e., the CCP and AMNC). Note that the error bars indicate the standard deviation.

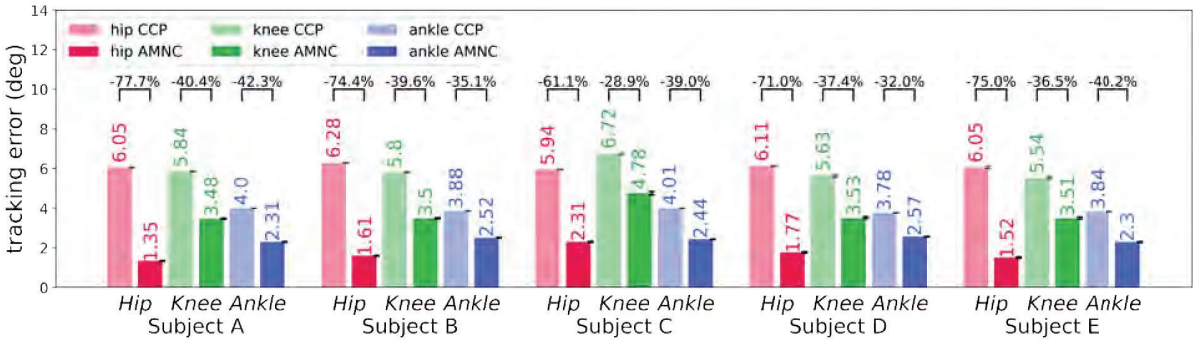

Fig. 7: Root-mean-square of the positional tracking error of different joints (i.e., hip, knee, and ankle), evaluated on five subjects under two controls (i.e., the CCP and AMNC). Note that the error bars indicate the standard deviation, and examples of time series plots are presented in Figs. S2–S4 in the supplementary material.

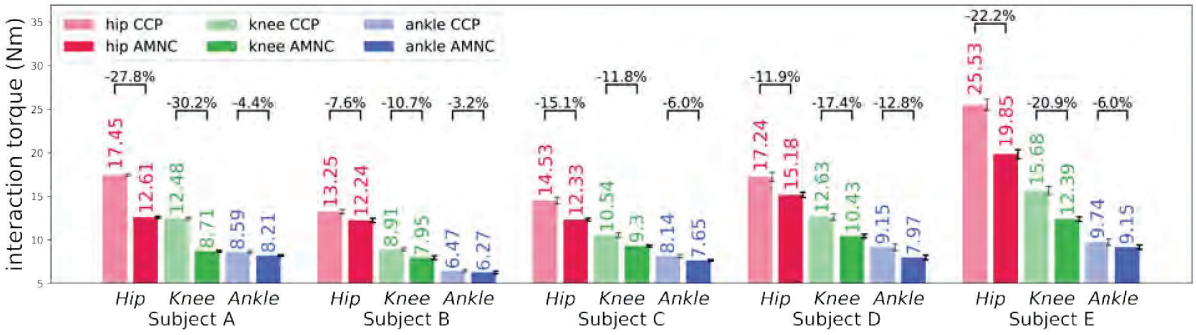

Fig. 8: Root-mean-square of the interaction torque of different joints (i.e., hip, knee, and ankle), evaluated on five subjects under two controls (i.e., the CCP and AMNC). Note that the error bars indicate the standard deviation, and examples of time series plots are present in Figs. S2–S4 in the supplementary material.

AMNC can continuously adapt the phase system on the fly by not only slowing the phase dynamics, such as phase-stopping DMP [21], but also accelerating the dynamics and synchronizing to the user's walking frequency. In addition, the trajectory shape changes as it deviates from the predetermined one and adapts to the user trajectory. Instead of utilizing historical trajectory information for gait prediction and adaptation [22], the AMNC exploits spontaneous trajectory information encoded in the RBF and corresponding GA networks to identify the proper adaptation direction, as illustrated in Figs. 3 and 4.

Although some methods can achieve both frequency/phase and shape synchronization/adaptation [5, 6, 8, 9] (refer to Table II), such as our AMNC, they still require some gait cycles for learning and adaptation; hence, they cannot be used instantly by new users. For example, the Bayesian optimization-based control, LINECOSPAR [5], took approximately 30 training trails ($\gg$ 30 gait cycles). Using the AFO-based control [6] took around 6 gait cycles to converge, while the PSAO-based control solely [8] or with an additional foot state signal in gait enhancing mechatronic system (GEMS) [9] took at least 4 gait cycles to converge.

Compared with all these, the AMNC adapts the signal shape and frequency online within a gait cycle (i.e., using sensory feedback and adaptation mechanisms to immediately adapt the next control command, as illustrated in Fig. S5); hence, the exoskeleton system implementing the AMNC can generalize and be applied to new users directly (i.e., new users can start walking with the exoskeleton without a training session).

TABLE II: Performance comparison between the state-of-the-art methods and the proposed AMNC in terms of shape adaptation, frequency/phase adaptation, online learning/adaptation, convergence, the ability to generalize to new users, the ability to generalize to different conditions (e.g., different slopes/terrains), and additional feedback (apart from joint position). Note that ✓, ●, and ✗ denote inclusion, partial inclusion (included in high-level environment recognition control), and exclusion, respectively. Details of the methods are summarized in Table SI in the supplementary material.

Methods	**shape adaptation**	**frequency/phase adaptation**	**online learning/adaptation**	**convergence* (gait cycles)**	**generalize to new users**	**generalize to different conditions (e.g., different slopes/terrains)**	**additional feedback (apart from joint position)**
LINECOSPAR [5]	✓	✓	✗	$\gg 30^p$	✗	✗	preference
AFO [6]	✓	✓	✓	$\approx 6^p$	✗	✗	-
FHAE [7]	✗	✓	✓	$\approx 3^p$	✗	✗	IMU
PSAO [8]	✓	✓	✓	$\approx 4^s$	✗	✗	-
GEMS [9]	✓	✓	✓	$\approx 6^p$	✗	●	foot state
DMP-HIL [10]	✓	✗	✓	$\approx 15^s$	✗	✗	-
DDOC [11]	✓	✗	✓	$\approx 4^p$	✗	✗	IMU
CCP-HIL [14]	✓	✗	✓	$\approx 10^p$	✗	✗	-
CCP [14]	✓	✗	✓	$\approx 0^p$	✓	✗	-
AMNC (OURS)	✓	✓	✓	$\approx 0^p$	✓	✓	-

* convergence is defined as the number of gait cycle that each method took to reach 80% of its maximum reported performance.
^{s} denotes the result obtained from simulation.
^{p} denotes the result obtained from the physical experiment.

Furthermore, when a user wears the exoskeleton implementing the AMNC, synchronization and adaptation are achieved without installing additional sensors, such as IMUs [7, 11, 22], foot state [9], or torque sensors [23], on either the user or exoskeleton. Only the feedback from positional encoders (mandatory sensors in robot control) is required to calculate the tracking error. By optimizing the tracking error and comparing the AMNC with the state-of-the-art CCP control, the AMNC can further reduce interaction torque, further lowering the force required by the user. This aspect would offer the opportunity to utilize redundancy sensory feedback (e.g., the control can operate with only positional feedback or torque feedback) to improve robustness, handle sensor malfunction, and ultimately guarantee the user's safety. In fact, the AMNC is not limited to level floor walking (as presented in the results above). It can also effectively assist a user in walking on different conditions (e.g., walking on a treadmill with varying slope angles, which has not been demonstrated by other methods [5–8, 10, 11, 14], see section SIV of the supplementary material and the video at https://youtu.be/BUSyHQ0Grf0).

Although the exoskeleton system has a relatively long transient response of approximately 0.2 s, exhibits a comparatively large discrete control/feedback resolution of 1^o, and is validated with noncompliance position control, the AMNC manages to achieve gait synchronization and locomotion assistance. However, the AMNC can adapt well in a specific range, as illustrated in Fig. 5. Further developments, such as employing compliance torque control [10, 14], assist-as-needed (AAN) control strategies [24], or efference copy signals with forward models [25], are expected to significantly improve the performance if implemented. Although our work demonstrates that the feedback from the hip and knee joints is sufficient for stable locomotion and gait adaptation on flat terrain and different slopes, walking on uneven terrain, which directly affects the ankle joints, may require ankle joint feedback for stable terrain adaptation [26]. Hence, this will be investigated further in the future.

VI. Acknowledgment

This study was supported by the Personalized lower-limb EXOskeleton with Versatility and Intelligence for clinical uSe (EXOVIS) project (Grant No. I20POM-INT010, https://brain.vistec.ac.th/research/projects/exovis-project/) [PM].

VII. Ethics Statement

The experiment in this study was approved by the Research Ethics Committee of the University of Southern Denmark (Case No. 20/70422).

VIII. Supplementary Materials

The supplementary video is at https://youtu.be/WwdrFzYO8fY, and the supplementary document is at https://github.com/Arthicha/EXOVIS_AMNC.

References

[1] Libo Zhou, Weihai Chen, Wenjie Chen, Shaoping Bai, Jianbin Zhang, and Jianhua Wang. Design of a passive lower limb exoskeleton for walking assistance with gravity compensation. *Mechanism and Machine Theory*, 150:103840, 2020.

[2] Nicholas A Bianco, Patrick W Franks, Jennifer L Hicks, and Scott L Delp. Coupled exoskeleton assistance simplifies control and maintains metabolic benefits: a simulation study. *bioRxiv*, 2021.

[3] Romain Baud, Ali Reza Manzoori, Auke Ijspeert, and Mohamed Bouri. Review of control strategies for

lower-limb exoskeletons to assist gait. *Journal of NeuroEngineering and Rehabilitation*, 18(1):1–34, 2021.

[4] Gian Maria Gasparri, Michael Owen Bair, Robert Patrick Libby, and Zachary Forest Lerner. Verification of a robotic ankle exoskeleton control scheme for gait assistance in individuals with cerebral palsy. In *2018 IEEE/RSJ International Conference on Intelligent Robots and Systems (IROS)*, pages 4673–4678. IEEE, 2018.

[5] Maegan Tucker, Myra Cheng, Ellen Novoseller, Richard Cheng, Yisong Yue, Joel W Burdick, and Aaron D Ames. Human preference-based learning for high-dimensional optimization of exoskeleton walking gaits. In *2020 IEEE/RSJ International Conference on Intelligent Robots and Systems (IROS)*, pages 3423–3430. IEEE, 2020.

[6] Hamidreza Talatian, Mohammad Karami, Hamed Moradi, and Gholamreza Vossoughi. Design and implementation of an intelligent control system for a lower-limb exoskeleton to reduce human energy consumption. In *2021 10th International Conference on Modern Circuits and Systems Technologies (MOCAST)*, pages 1–4. IEEE, 2021.

[7] Tao Xue, Ziwei Wang, Tao Zhang, and Meng Zhang. Adaptive oscillator-based robust control for flexible hip assistive exoskeleton. *IEEE Robotics and Automation Letters*, 4(4):3318–3323, 2019.

[8] Keehong Seo, SeungYong Hyung, Byung Kwon Choi, Younbaek Lee, and Youngbo Shim. A new adaptive frequency oscillator for gait assistance. In *2015 IEEE International Conference on Robotics and Automation (ICRA)*, pages 5565–5571. IEEE, 2015.

[9] Keehong Seo, Kyungrock Kim, Young Jin Park, Joon-Kee Cho, Jongwon Lee, Byungjune Choi, Bokman Lim, Younbaek Lee, and Youngbo Shim. Adaptive oscillator-based control for active lower-limb exoskeleton and its metabolic impact. In *2018 IEEE International Conference on Robotics and Automation (ICRA)*, pages 6752–6758. IEEE, 2018.

[10] Rui Huang, Hong Cheng, Hongliang Guo, Xichuan Lin, and Jianwei Zhang. Hierarchical learning control with physical human-exoskeleton interaction. *Information Sciences*, 432:584–595, 2018.

[11] Zhinan Peng, Rui Luo, Rui Huang, Tengbo Yu, Jiangping Hu, Kecheng Shi, and Hong Cheng. Data-driven optimal assistance control of a lower limb exoskeleton for hemiplegic patients. *Frontiers in Neurorobotics*, 14:37, 2020.

[12] Shiyin Qiu, Wei Guo, Darwin Caldwell, and Fei Chen. Exoskeleton online learning and estimation of human walking intention based on dynamical movement primitives. *IEEE Transactions on Cognitive and Developmental Systems*, 13(1):67–79, 2020.

[13] Andres Martinez, Brian Lawson, Christina Durrough, and Michael Goldfarb. A velocity-field-based controller for assisting leg movement during walking with a bilateral hip and knee lower limb exoskeleton. *IEEE Transactions on Robotics*, 35(2):307–316, 2018.

[14] Rui Huang, Hong Cheng, Jing Qiu, and Jianwei Zhang. Learning physical human–robot interaction with coupled cooperative primitives for a lower exoskeleton. *IEEE Transactions on Automation Science and Engineering*, 16(4):1566–1574, 2019.

[15] Robotic Exoskeleton Exo-H3 Technaid—Leading Motion. https://www.technaid.com/, 2021. accessed: 2021-08-07.

[16] Frank Pasemann, Manfred Hild, and Keyan Zahedi. SO(2)-networks as neural oscillators. In *International Work-Conference on Artificial Neural Networks*, pages 144–151. Springer, 2003.

[17] Mathias Thor, Tomas Kulvicius, and Poramate Manoonpong. Generic neural locomotion control framework for legged robots. *IEEE transactions on neural networks and learning systems*, 32(9):4013–4025, 2020.

[18] Sebastian Ruder. An overview of gradient descent optimization algorithms. *arXiv preprint arXiv:1609.04747*, 2016.

[19] Emre Sariyildiz and Hakan Temeltas. Performance analysis of numerical integration methods in the trajectory tracking application of redundant robot manipulators. *International Journal of Advanced Robotic Systems*, 8(5):63, 2011.

[20] E. Rohmer, S. P. N. Singh, and M. Freese. V-rep: A versatile and scalable robot simulation framework. In *2013 IEEE/RSJ International Conference on Intelligent Robots and Systems*, pages 1321–1326, 2013. doi: 10.1109/IROS.2013.6696520.

[21] Auke Jan Ijspeert, Jun Nakanishi, and Stefan Schaal. Movement imitation with nonlinear dynamical systems in humanoid robots. In *Proceedings 2002 IEEE International Conference on Robotics and Automation (Cat. No. 02CH37292)*, volume 2, pages 1398–1403. IEEE, 2002.

[22] Zhenlei Chen, Qing Guo, Tieshan Li, Yao Yan, and Dan Jiang. Gait prediction and variable admittance control for lower limb exoskeleton with measurement delay and extended-state-observer. *IEEE Transactions on Neural Networks and Learning Systems*, 2022.

[23] Yi Long, Zhi-jiang Du, Wei-dong Wang, and Wei Dong. Human motion intent learning based motion assistance control for a wearable exoskeleton. *Robotics and Computer-Integrated Manufacturing*, 49:317–327, 2018.

[24] Lincong Luo, Liang Peng, Chen Wang, and Zeng-Guang Hou. A greedy assist-as-needed controller for upper limb rehabilitation. *IEEE transactions on neural networks and learning systems*, 30(11):3433–3443, 2019.

[25] Jettanan Homchanthanakul and Poramate Manoonpong. Continuous online adaptation of bioinspired adaptive neuroendocrine control for autonomous walking robots. *IEEE Transactions on Neural Networks and Learning Systems*, 33(5):1833–1845, 2021.

[26] Adriana Torres-Pardo, David Pinto-Fernández, Manolo Garabini, Franco Angelini, David Rodriguez-Cianca, Stefano Massardi, Jesús Tornero-López, Juan C Moreno, and Diego Torricelli. Legged locomotion over irregular terrains: State of the art of human and robot performance. *Bioinspiration & Biomimetics*, 2022.